Electronic Supplementary Information

Homologue-paired liquids as special non-ionic deep eutectic solvents for efficient absorption of SO$_2$

Hangzhi Wu, [a, b] Wenjie Xiong, [b] Shuyue Wen, [b] Xiaomin Zhang, [b, c]* Shule Zhang [a]*

[a] School of Chemistry and Chemical Engineering, Nanjing University of Science and Technology, Nanjing 210094, PR China

[b] Key Laboratory of Mesoscopic Chemistry of MOE, School of Chemistry and Chemical Engineering, Nanjing University, Nanjing 210023, P.R. China.

[c] Yuxiu Postdoctoral Institute, Nanjing University, Nanjing 210023, P. R. China.

Email: xmzhang@nju.edu.cn; shulezhang@163.com;

General Information

N$_2$ (99.99 mol%) and SO$_2$ (99.9 mol%) were provided by Jiangsu Tianhong Chemical Co., Ltd. Acetamide (99 wt%), 1,3-dimethyl-2-imidazolidinone (99 wt%), and tetramethylurea (99 wt%) were purchased from Aladdin Reagents (Shanghai) Co., Ltd. Imidazole (99 wt%) was obtained from Sinopharm Chemical Reagent Co., Ltd. 2-Pyrrolidinone (98 wt%) and 2-imidazolidone (98 wt%) were purchased from Saen Chemical Technology (Shanghai) Co., Ltd. N-methyl-2-pyrrolidinone (99 wt%) and 1-Ethylimidazole (99 wt%) were provided by Shanghai Adamas Reagents Co., Ltd. N-methylacetamide (> 99 wt%) was obtained from Meryer (Shanghai) Chemical Technology Co. Ltd. N, N'-Dimethylurea was purchased from Nine-Dinn Chemistry (Shanghai) Co., Ltd.

The density were determined using an Anton Paar DMA 5000 densiometer with a precision of 0.00001 g·cm^{-3}, which was calibrated using distilled water at desired

temperature. Viscosity was measured on a Brookfield DV2TLV viscometer equipped with a spindle CPA-41Z (viscosity ranges from 0.58 to 11510 mPa·s). The rotational speed (N) of the spindle ranges from 0.1 to 200 rpm and the shear rate of the spindle is $2.0N \text{ s}^{-1}$. The uncertainty of the viscometer is ±1% in relation to the full scale. Thermal gravity (TG) traces were recorded on a PerkinElmer Pyris 1 TGA from room temperature to 573 K with a scanning rate of 10 K·min^{-1} under N_2 atmosphere. Fourier Transform Infrared (FTIR) spectra were obtained on a Nicolet iS50 infrared spectrometer. The Bruker DPX 400 MHz spectrometer was used to conduct the Nuclear Magnetic Resonance (NMR) characterization with d$_6$-DMSO as solvent.

The verification of the formation of hydrogen bonds between HBD and HBA by gaussian calculation

To prove the formation of hydrogen bonds between HBD and HBA, the optimized structures of Eim-Eim, Im-Im, and Eim-Im (1:1) are obtained at B3LYP/ 6-311g(d,p) level by Gaussian calculations based on the density functional theory, and so does it for NMP-2-Pyr system (**Fig. S1–S6**). The enthalpy change and Gibbs free energy change of the mixing process are calculated using **Equations S1** and **S2**. It is found that the enthalpy changes of NMP-2-Pyr and Eim-Im systems are −10.1 and −26.1 kJ·mol^{-1}, respectively, indicating an exothermic mixing process. The free energy changes of the two systems are −12.2 and −26.9 kJ·mol^{-1}, respectively, demonstrating a spontaneous mixing behavior and also the formation of hydrogen bonds between the homologues.
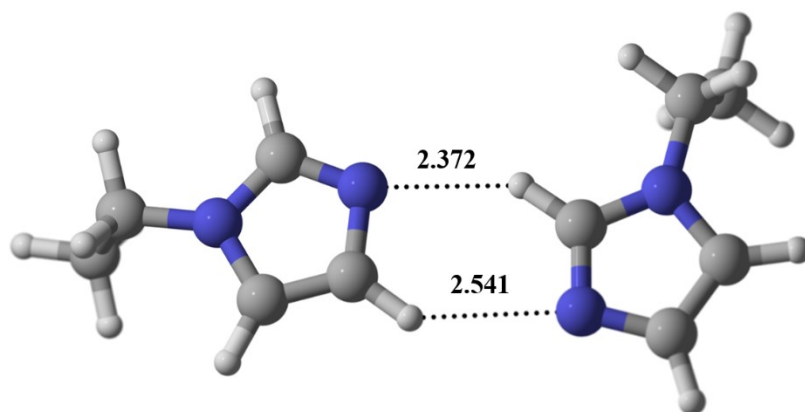
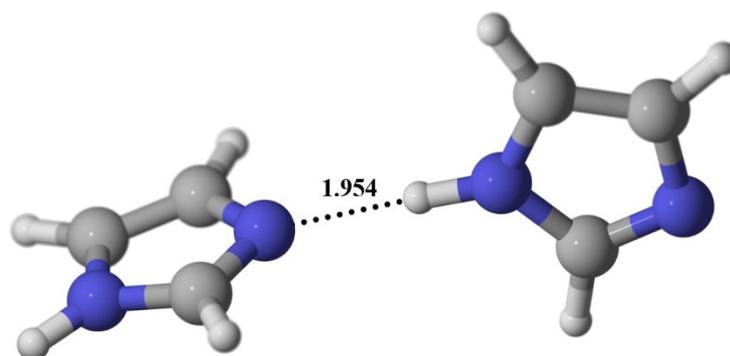**Fig. S1** Optimized structure of Eim-Eim obtained by B3LYP/ 6-311g(d,p).

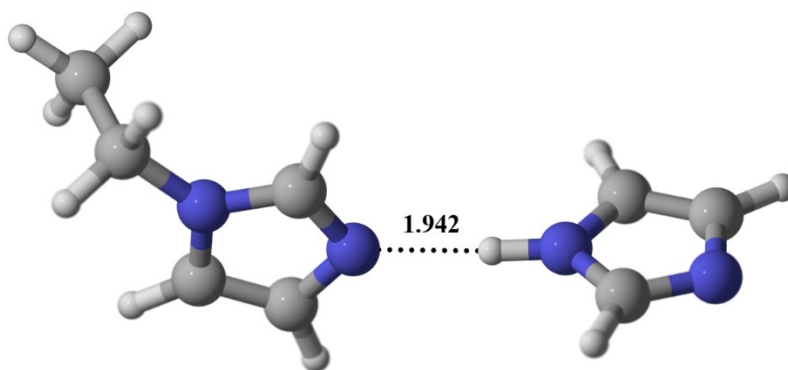**Fig. S2** Optimized structure of Im-Im obtained by B3LYP/ 6-311g(d,p).

Fig. S3 Optimized structure of Eim-Im obtained by B3LYP/ 6-311g(d,p).
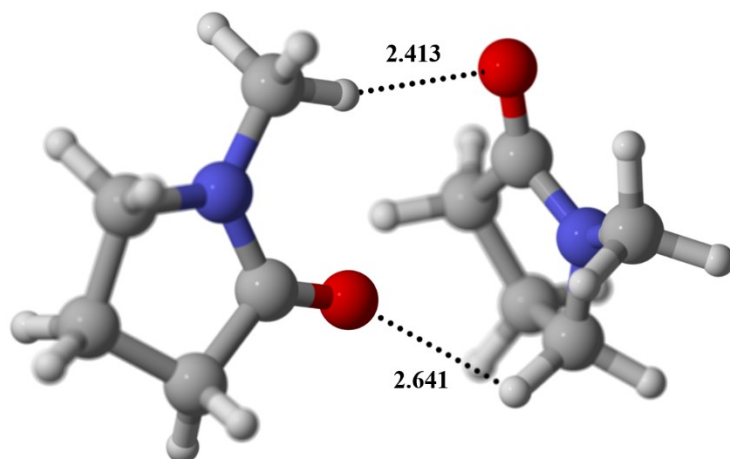
Fig. S4 Optimized structure of NMP-NMP obtained by B3LYP/ 6-311g(d,p).
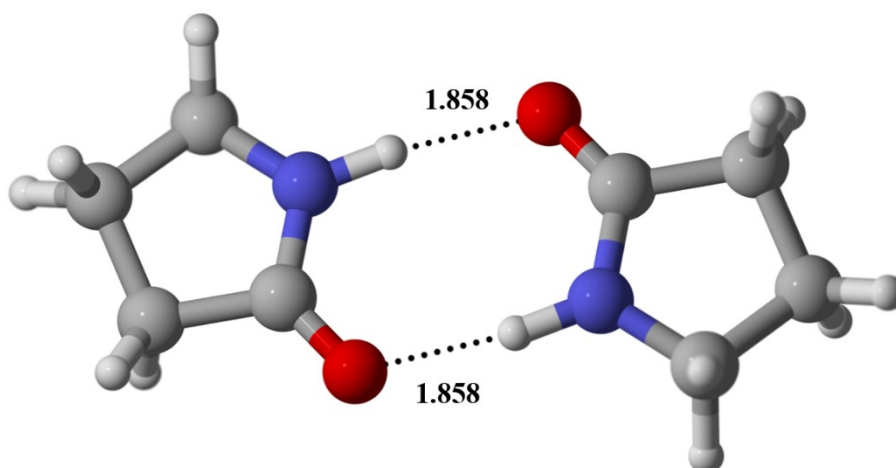

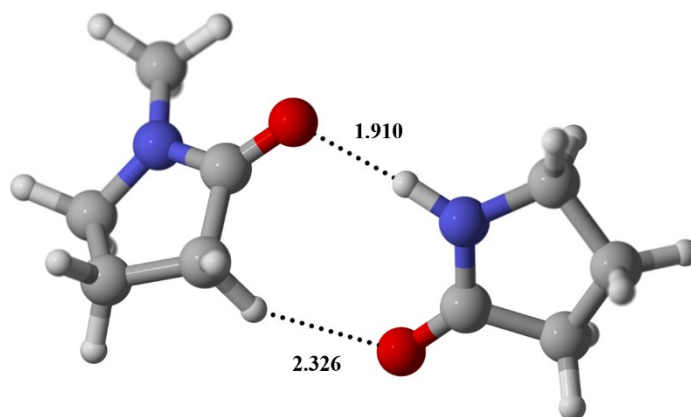**Fig. S5** Optimized structure of 2-Pyr-2-Pyr obtained by B3LYP/ 6-311g(d,p).

Fig. S6 Optimized structure of NMP-2-Pyr obtained by B3LYP/ 6-311g(d,p).

Calculation of enthalpy changes and Gibbus free energy change of mixing process

$$\Delta H_{mix} = 2H_{A-B} - H_{A-A} - H_{B-B} \qquad (S1)$$

Where ΔH_{mix} represents the enthalpy change of mixing process, H_{A-B}, H_{A-A}, and H_{B-B} denote the enthalpy of A-B complex, A-A complex, and B-B complex, respectively.

$$\Delta G_{mix} = 2G_{A-B} - G_{A-A} - G_{B-B} \qquad (S2)$$

Where ΔG_{mix} represents the enthalpy change of mixing process, G_{A-B}, G_{A-A}, and G_{B-B} denote the Gibbs free energy change of A-B complex, A-A complex, and B-B complex, respectively.
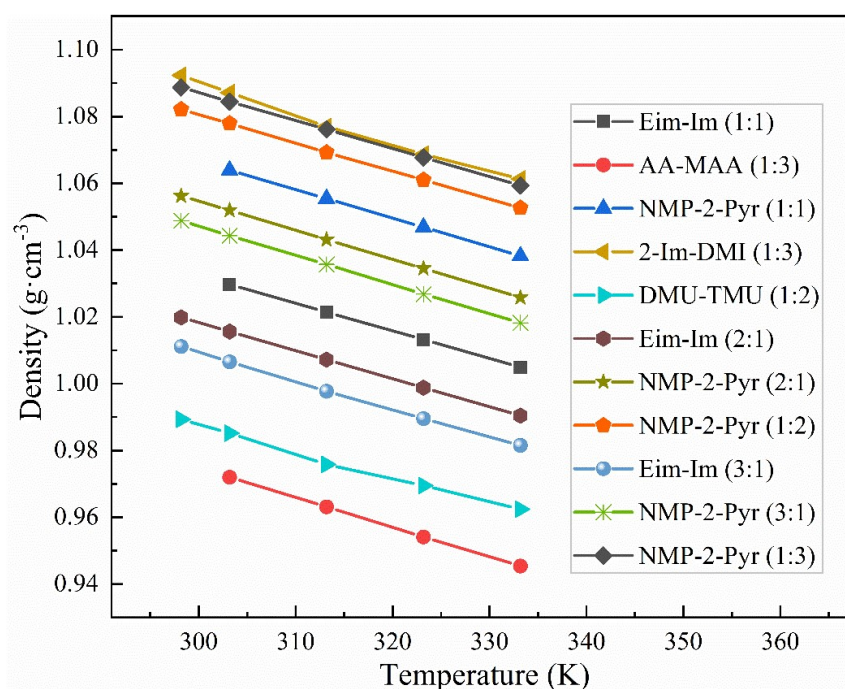

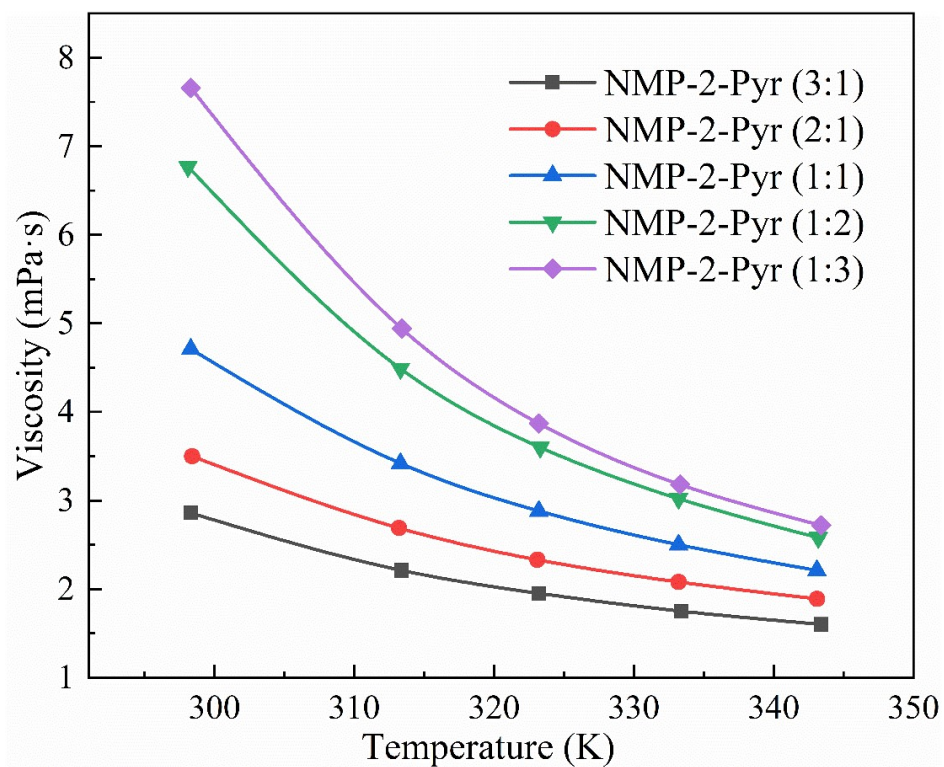**Fig. S7** Density of HPLs as a function of temperature.

Fig. S8 Viscosity of NMP-2-Pyr systems as a function of temperature.
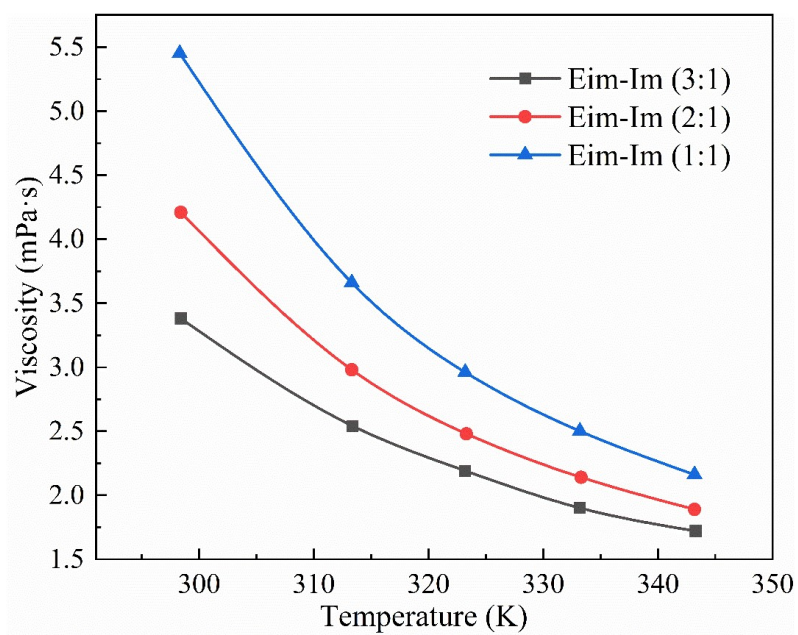

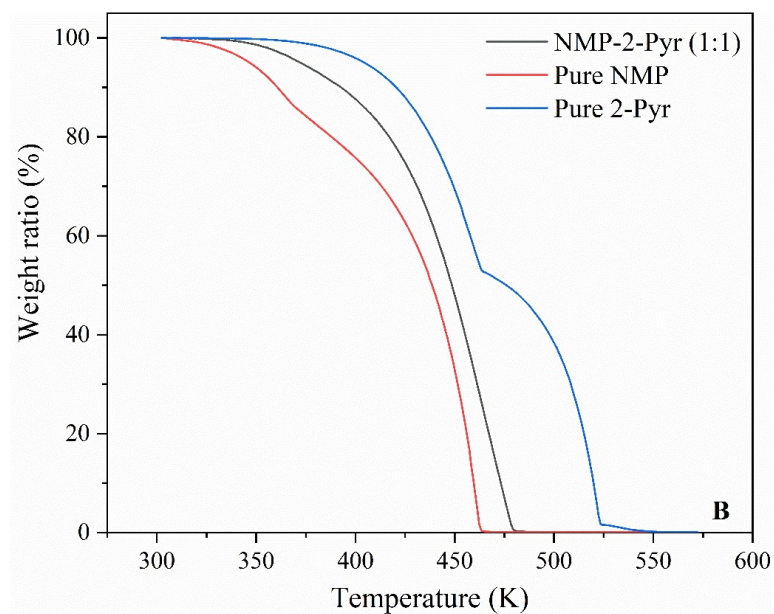**Fig. S9** Viscosity of Eim-Im systems as a function of temperature.

Fig. S10 The TGA curves of pure NMP, pure 2-Pyr, and NMP-2-Pyr (1:1).
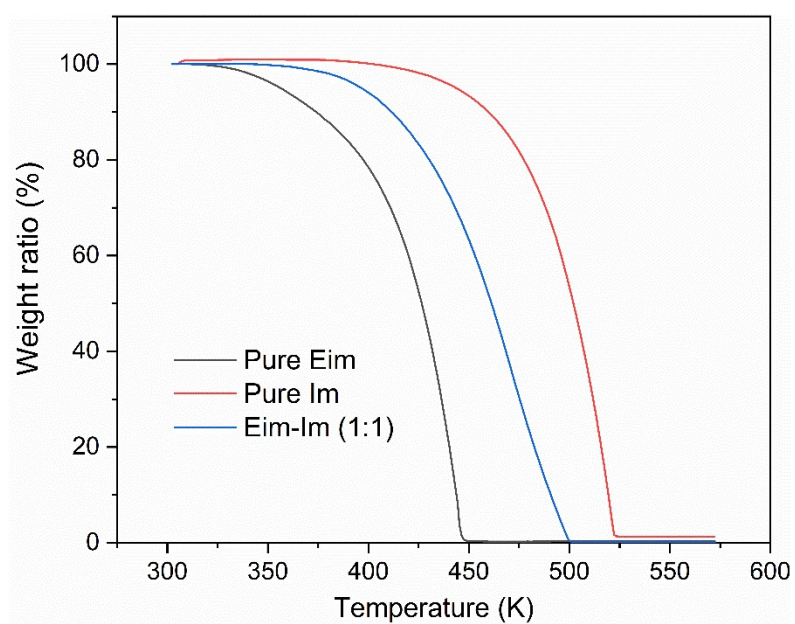
Fig. S11 The TGA curves of pure Eim, pure Im, and Eim-Im (1:1).
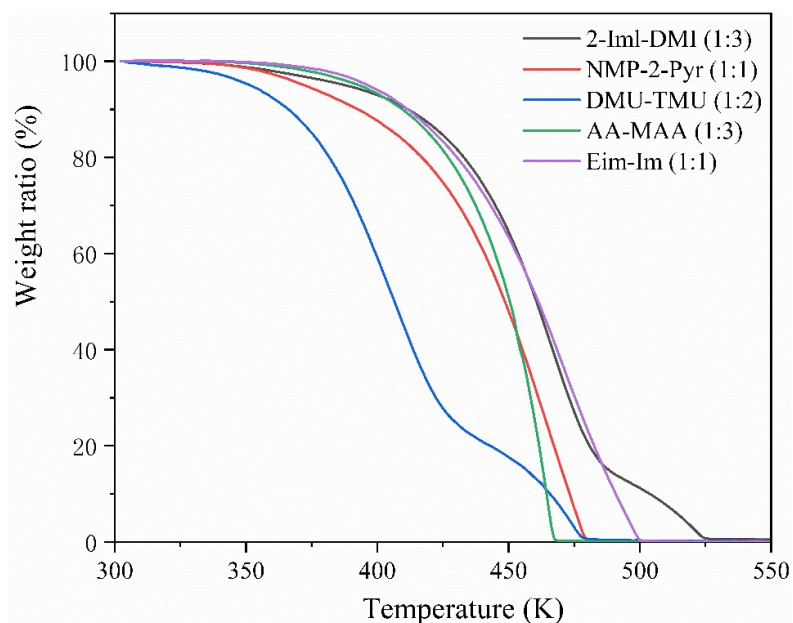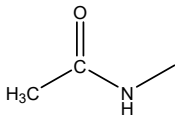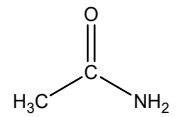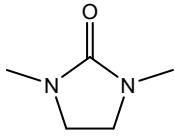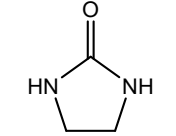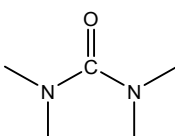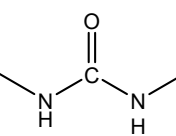
Fig. S12 The TGA curves of five typical HPLs.

Table S1. A summary of boiling and melting points of components, and melting points

of five typical HPLs

Name	Chemical structures		Boiling point (K)		Melting point (K)		Melting point
	HBA	HBD	HBA	HBD	HBA	HBD	of HPL (K)
Eim-Im (1:1)			499	530	NA	363	178
NMP-2-Pyr (1:1)			475	518	249	298	NA

MAA-AA (3:1)	(structure: N-methylacetamide)	(structure: acetamide)	478	494	304	354	281/287
DMI-2-Iml (3:1)	(structure: DMI)	(structure: 2-imidazolidinone)	498	436[a]	281	403	246/266
TMU- DMU (1:2)	(structure: tetramethylurea)	(structure: dimethylurea)	448	542	272	375	258

NA: not available; [a] at 0.4 kPa

Fig. S13 DSC curves of seven typical HPLs.

Measurement of saturated vapor pressure

The saturated vapor pressure of NMP-2-Pyr system was measured by a home-made

equipment. A chamber whose volume is about 40 cm^3 is equipped with a magnetic stirrer to be as equilibrium cell. The temperatures (T) of the chamber is controlled by oil bath with an uncertainty of ±0.1 K. The pressure is monitored using a pressure transducer of ±0.2% uncertainty (in relation to the full scale), which is connected to a Numeric Instrument to record the pressure changes online. In a typical absorption, a known mass (about 1.0 g) of sample was placed into the chamber, and then the air in the chamber was evacuated at room temperature. Equilibrium was thought to be reached when the pressure of the chamber remained constant for 4 hours at 403.2 K.
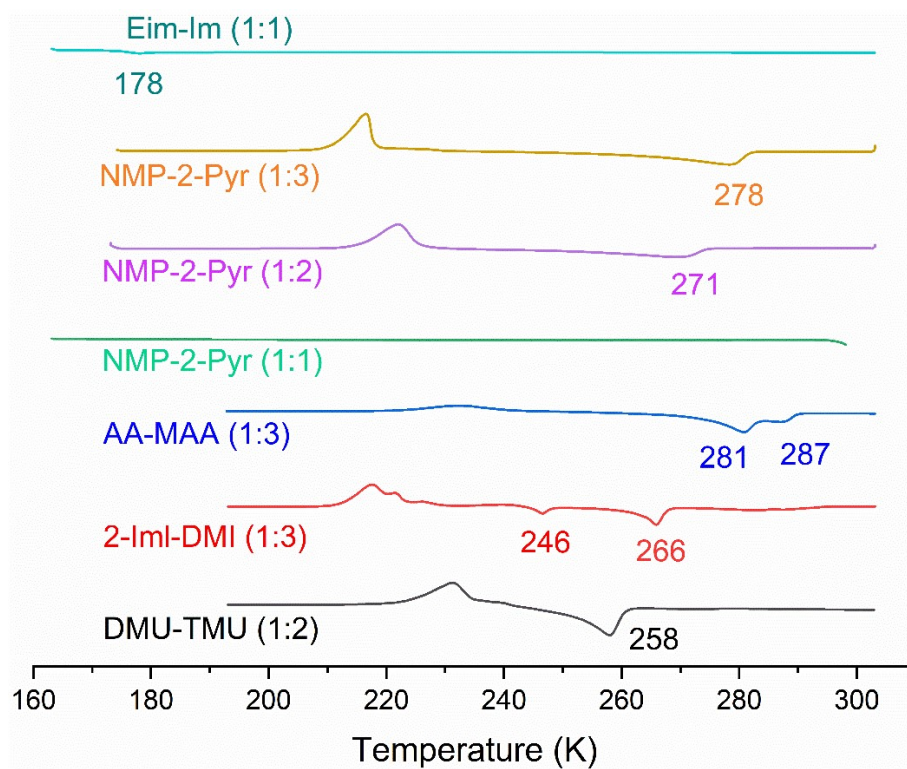
Method of absorption experiments

The absorption of SO_2 were carried out using well-defined process according to literatures. The whole device consists of two glass chambers whose volumes are 189.9 cm3 (V_1) and 40.16 cm^3 (V_2), respectively. The bigger chamber, named as gas reservoir, isolates gas before it contacts the liquid samples in the smaller chamber. The smaller chamber used as equilibrium cell is equipped with a magnetic stirrer. The temperatures (T) of both chambers are controlled by a water bath with an uncertainty of ±0.1 K. The pressures in the two chambers are monitored using two pressure transducers of ±0.2% uncertainty (in relation to the full scale). The pressure transducers are connected to a Numeric Instrument to record the pressure changes online.

In a typical run, a known mass (w) of pure HPL sample was placed into the equilibrium cell, and the air in the two chambers was evacuated. The pressure in the equilibrium cell was recorded to be P_0. Desired gas from gas cylinder was then fed into the gas reservoir to a pressure of P_1. The needle valve between the two chambers was turned on to let the acidic gas be introduced to the equilibrium cell. Absorption

equilibrium was thought to be reached when the pressures of the two chambers remained constant for at least 1 h. The equilibrium pressures were denoted as P_2 for the equilibrium cell and P'_1 for the gas reservoir. The gas partial pressure in the equilibrium cell was $P_S = P_2 - P_0$. The acidic gas absorption capacity, $n(P_S)$, can thus be calculated using the following equation:

$$n(P_s) = \rho_g(P_1,T)V_1 - \rho_g(P'_1,T)V_1 - \rho_g(P_s,T)(V_2 - \omega/\rho_{HPL}) \quad (S3)$$

where $\rho_g(P_i,T)$ represents the density of gas in mol·cm^{-3} at P_i (i = 1, S) and T; ρ_{HPL} is the density of HPL in g·cm^{-3} at desired temperature. V_1 and V_2 represent the volumes in cm^3 of the two chambers, respectively. After determinations, SO_2 left in the chambers was introduced to an off-gas absorber containing aqueous solution of NaOH in order to prevent SO_2 leaking into the atmosphere. Duplicate experiments for each sample were preformed to obtain the averaged values of gas solubility.
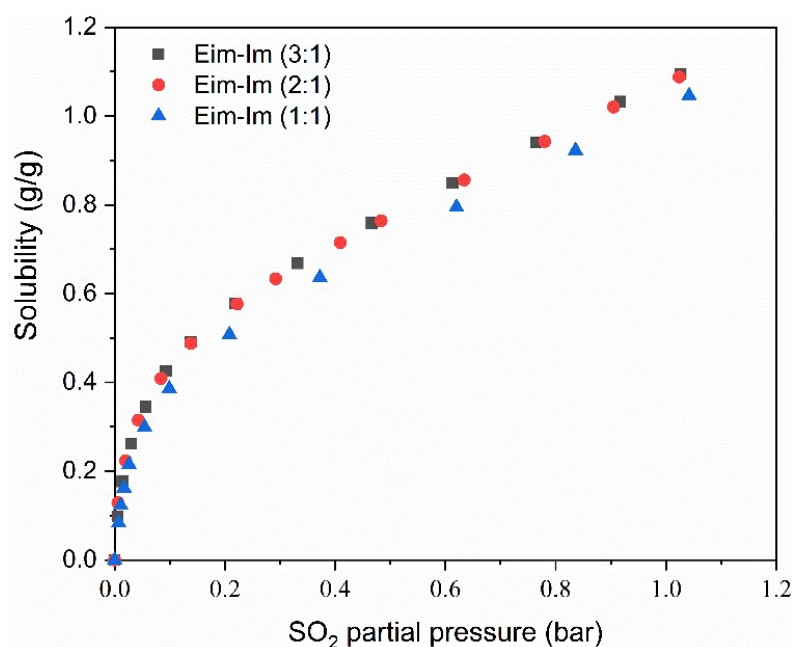

Fig. S14 The solubility of SO_2 in Eim-Im system as function of composition at 298.2 K.
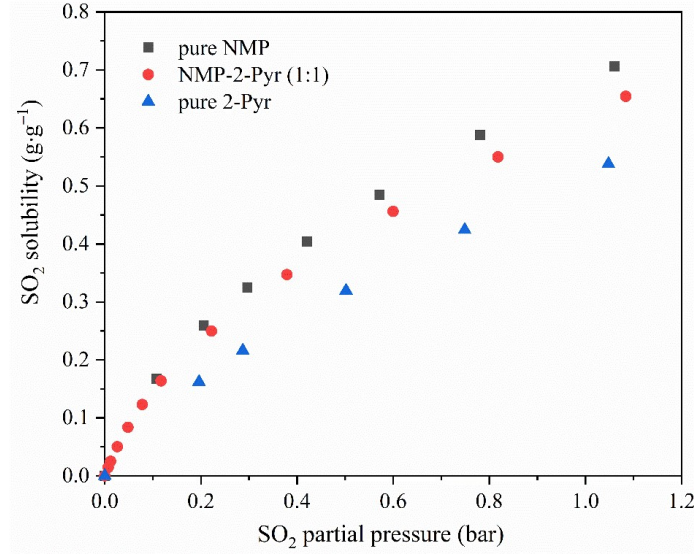
Fig. S15 The solubility of SO_2 in pure NMP, NMP-2-Pyr (1:1), and pure 2-Pyr at 313.2 K.

Development of RETM model

Assuming that 1 mole of SO_2 reacts with 1mole of NMP-2-Pyr (1:1), the reaction of SO_2 with the HPL can be given as:

$$SO_2(g) \rightarrow SO_2(l) \tag{S4}$$

$$SO_2(l) + HPL(l) \rightarrow SO_2 - HPL(l) \tag{S5}$$
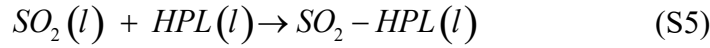
Combining equation (S4) and (S5) leads to the overall reaction Equation (S6).

$$SO_2(g) + HPL(l) \rightarrow SO_2 - HPL(l) \tag{S6}$$
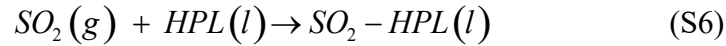
where g and l represent gas phase and liquid phase, respectively.

The Henry's law for the physical dissolution of SO_2 in dilute solution is defined in molality and given by Equation (S7).

$$P = H\gamma_{SO_2} \frac{m_{SO_2}}{m°} \tag{S7}$$

where P reprents the SO_2 partial pressure in bar, H is the Henry's constant in bar, and m_{SO_2} is the concentration of free SO_2 in mol·kg^{-1}.

The chemical equilibrium of Equation (S5) is expressed into Equation (S8), where K_1° denotes the equilibrium constant, γ_{SO_2}, γ_{HPL}, and γ_{SO_2-HPL} represent the activity coefficients of the physically dissolved SO_2, free HPL and SO_2-HPL complex in the HPL phase, respectively. m_{HPL} and m_{SO_2-HPL} are the concentrations of the HPL and the SO_2-HPL complex in mol·kg^{-1} and m° is the standard molality (1 mol·kg^{-1}). Similarly, the overall reaction equilibrium corresponding to Equation (S6) is formulated using Equation (S9), where K° is the equilibrium constant of the overall reaction and P° is the standard pressure (1.0 bar). Equation (S10) denotes the material conservation of the HPL, where m_{HPL_0} is the initial concentration of NMP-2-Pyr (1:1) that can be calculated from Equation (S11). M_{HPL} is the molecular weight of the HPL in g·mol^{-1}. The material conservation of SO_2 can be calculated by Equation (S12), where m_t is the total concentration of SO_2 in the HPL phase in the unit of mol·kg^{-1}.

$$K_1^\circ = \frac{\gamma_{SO_2-HPLs} \dfrac{m_{SO_2-HPLs}}{m^\circ}}{\gamma_{SO_2} \dfrac{m_{SO_2}}{m^\circ} \gamma_{HPLs} \dfrac{m_{HPLs}}{m^\circ}} \tag{S8}$$

$$K^\circ = \frac{\gamma_{SO_2-HPLs} \dfrac{m_{SO_2-HPLs}}{m^\circ}}{\dfrac{P}{P^\circ} \gamma_{HPLs} \dfrac{m_{HPLs}}{m^\circ}} \tag{S9}$$

$$m_{HPL_0} = m_{HPL} + m_{SO_2-HPLs} \tag{S10}$$

$$m_{HPL_0} = \frac{1000}{M_{HPL}} \tag{S11}$$

$$m_t = m_{SO_2} + m_{SO_2-HPLs} \tag{S12}$$

Combining Equation (S7), (S8) and (S9) results in Equation (S13):

$$K^\circ = \frac{K_1^\circ}{H} P^\circ \tag{S13}$$

The activity coefficients of these species can hardly be calculated becacuse of the absence of relevant thermodynamics parameters. They will be normalized in ideal diluted solution in the presence of low-concentration free SO_2. Therefore, it should be assumed that the product of three activity coefficients in Equations (S8) and (S9) is constant during the whole absorption process to simplify the equalibrum system. After deduction, equation (S14) is achieved to relate the total SO_2 solubility.

$$m_t = \left(\frac{m_{HPL_0}}{P + \dfrac{H}{K_1{}^\circ}} + \frac{1}{H} \right) P \tag{S14}$$

The enthalpy change of SO_2 absorption, ΔH, can be calculated using the Van't Hoff equation,

$$\frac{d \ln K_1{}^\circ}{d(1/T)} = -\frac{\Delta H}{R} \tag{S15}$$

Table S2. Fitting parameters of RETM for NMP-2-Pyr (1:1) + SO_2 system.

Temperature (K)	H / bar	$K_1{}^\circ$ / kg·mol^{-1}	R^2
298.2	0.1120 ± 0.0002	1.0495 ± 0.0093	0.9999
313.2	0.1918 ± 0.0011	0.9156 ± 0.0182	0.9999
323.2	0.2715 ± 0.0032	0.6965 ± 0.0214	0.9997
333.2	0.3748 ± 0.0065	0.6615 ± 0.0260	0.9997

Table S3. Fitting parameters of RETM for Eim-Im (1:1) + SO_2 system.

Temperature (K)	H / bar	$K_1{}^\circ$ / kg·mol^{-1}	R^2
298.2	0.0996 ± 0.0009	4.0540 ± 0.3028	0.9989

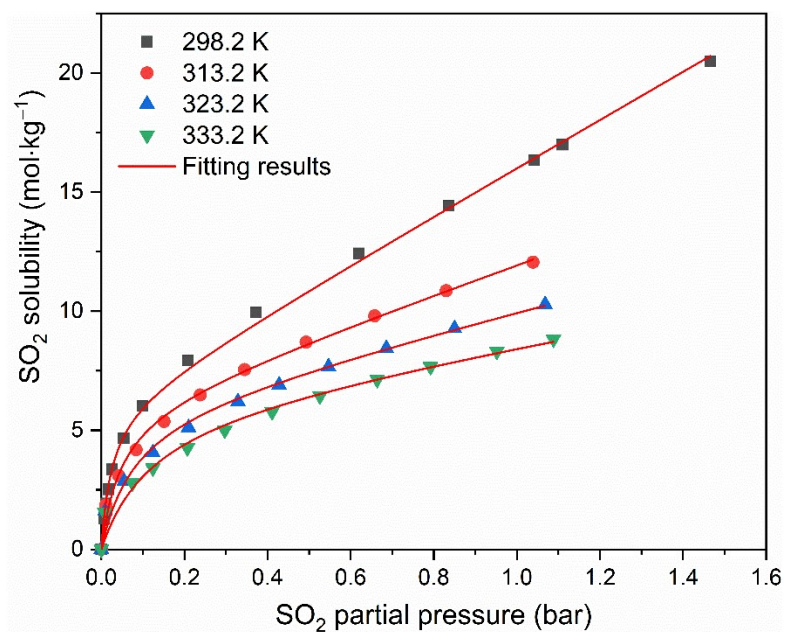|			
313.2	0.1643 ± 0.0045	3.5277 ± 0.0387	0.9962
323.2	0.2349 ± 0.0127	3.0061 ± 0.5117	0.9906
333.2	0.3374 ± 0.0291	2.7839 ± 0.5813	0.9822

Fig. S16 Temperature dependence of SO_2 solubility in Eim-Im (1:1).
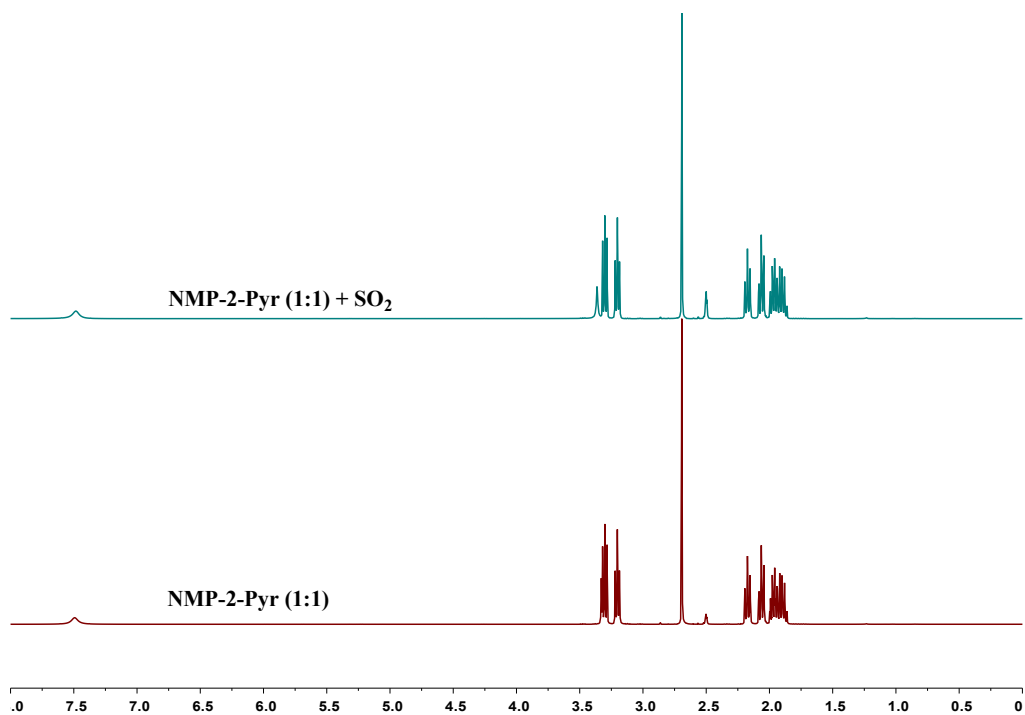
Fig. S17 ^{1}H NMR of NMP-2-Pyr (1:1) after and before SO_2 dissolution.
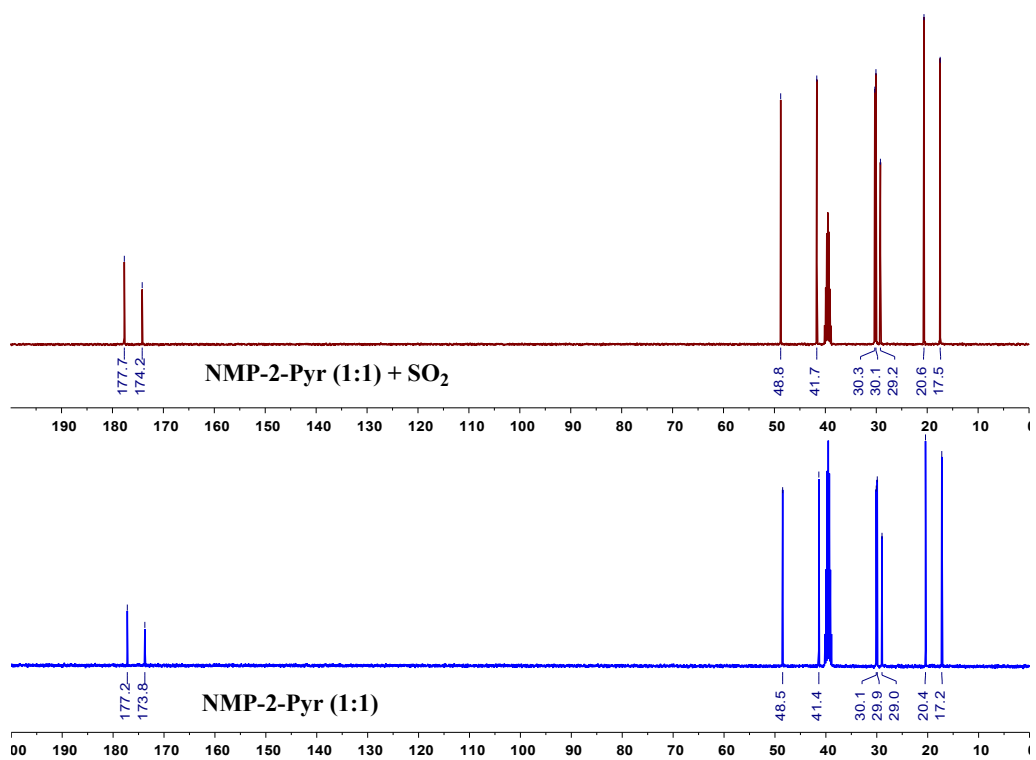

Fig. S18 ^{13}C NMR of NMP-2-Pyr (1:1) after and before SO_2 dissolution.
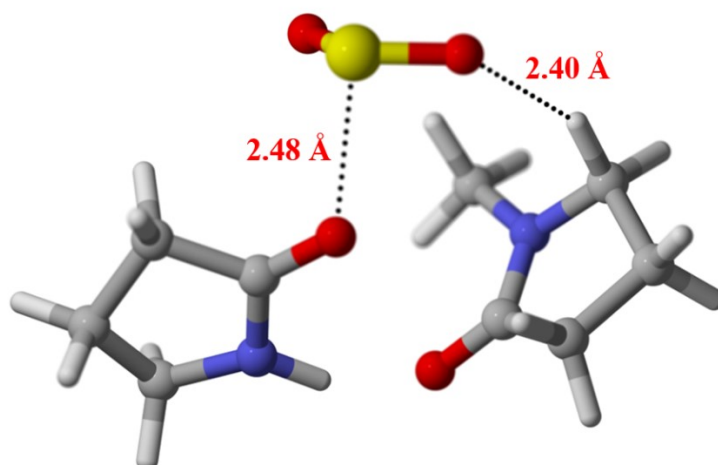
Fig. S19 Optimized structure of NMP-2-Pyr (1:1) + SO$_2$ obtained by B3LYP/6-311g (d, p).

The SO$_2$ absorption mechanism by Eim-Im (1:1)

We have carried out the NMR and FT-IR before and after SO$_2$ absorption of Eim-Im (1:1). As is shown in Fig. R6, the new peak at 525 cm^{-1} can be assigned to the scissor bending vibration (δ) of dissolved SO$_2$. In addition, the peaks between 1000 and 1150 cm^{-1} widen significantly and the peaks at 1138 and 1168 cm^{-1} are combined into one at 1146 cm^{-1} after SO$_2$ absorption. The above changes of peaks can be attributed to the appearance of S=O bond.[1-3] Additionally, the peaks at 1354 and 1393 cm^{-1} disappear after SO$_2$ capture. All the above evidence illustrates the chemical interaction of SO$_2$ with Eim-Im (1:1).

Fig. S20 FT-IR of Eim-Im (1:1) before and after the absorption of SO_2.

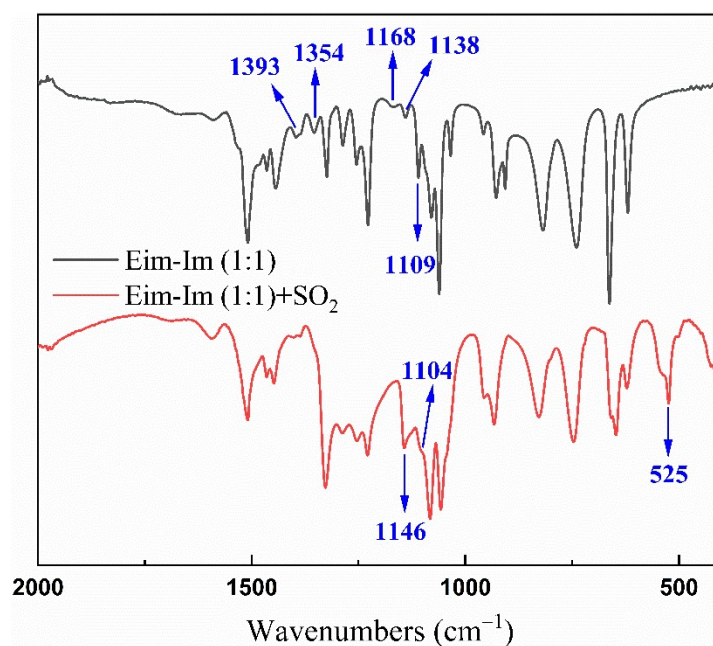Fig. R7-R8 show the NMR spectra of Eim-Im (1:1) before and after SO_2 capture. The chemical shifts of the H atoms connected to C(1) and C(2) on Im move upfield from 7.35 and 7.91 ppm to 7.26 and 8.00 ppm, respectively. Simultaneously, the chemical shifts of the C(1) and C(2) atoms on Im rise upfield from 122.2 and 135.8 ppm to 120.8 and 134.5 ppm, respectively. ^{1}H NMR and ^{13}C NMR demonstrate the direct interaction between Im and SO_2. For Eim, the chemical shifts of the H atoms connected to C(3), C(4), and C(5) on Eim move from 8.08, 7.24, and 7.38 ppm to 8.16, 7.11, and 7.27 ppm, respectively. Meanwhile, the chemical shifts of C(3), C(4), and C(5) atoms on Eim change upfield from 137.1, 128.7, and 119.3 ppm to 135.9, 125.9, and 119.8 ppm, respectively. ^{1}H NMR and ^{13}C NMR also demonstrate the direct interaction between Eim and SO_2. Consequently, it is concluded that there exists acid-base chemical interaction between SO_2 and Im as well as SO_2 and Eim based on the characterization data. Thus, the absorption mechanism of SO_2 by Eim-Im (1:1) is proposed in Scheme S1.
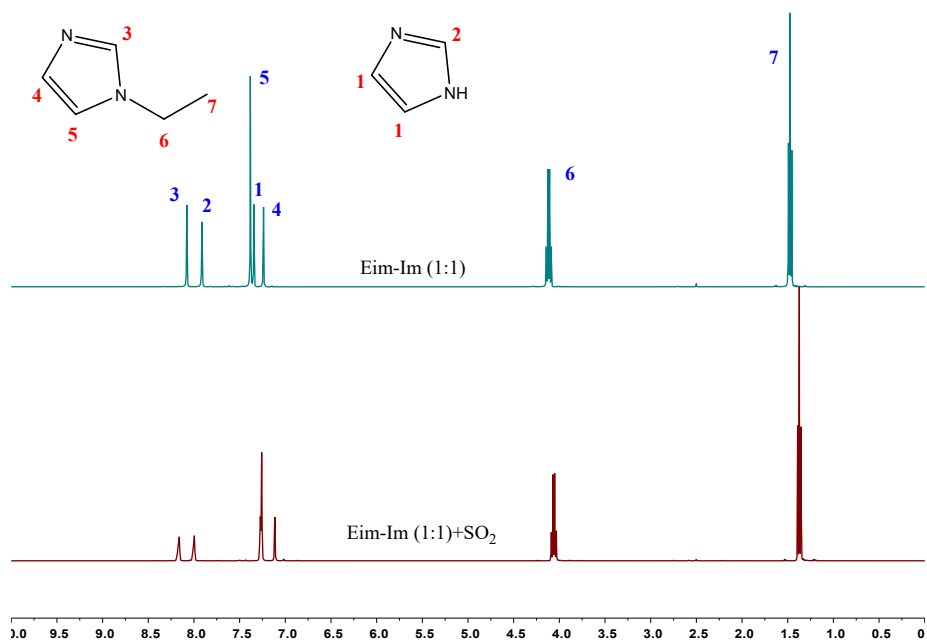
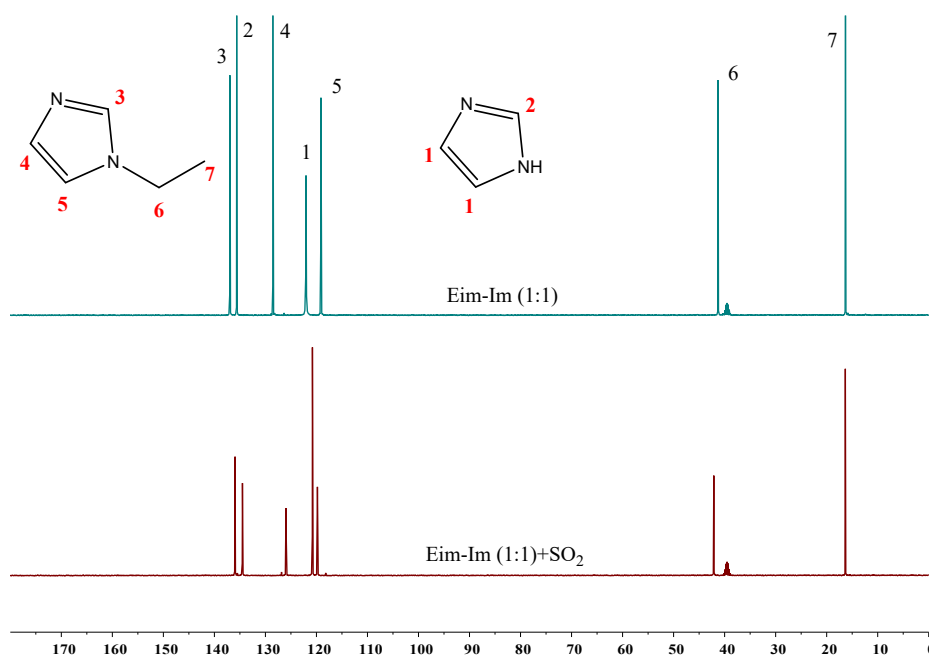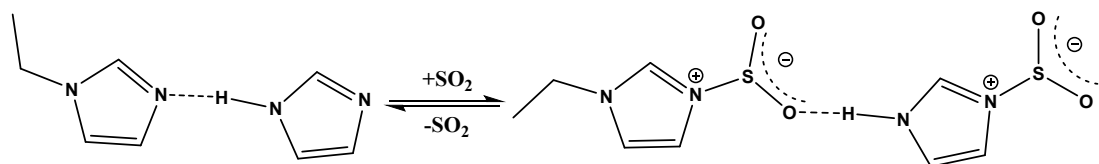**Fig. S21** ^{1}H NMR of Eim-Im (1:1) before and after the absorption of SO$_2$.

Fig. S22 ^{13}C NMR of Eim-Im (1:1) before and after the absorption of SO$_2$.

Scheme S1. The proposed absorption mechanism between Eim-Im (1:1) and SO$_2$.
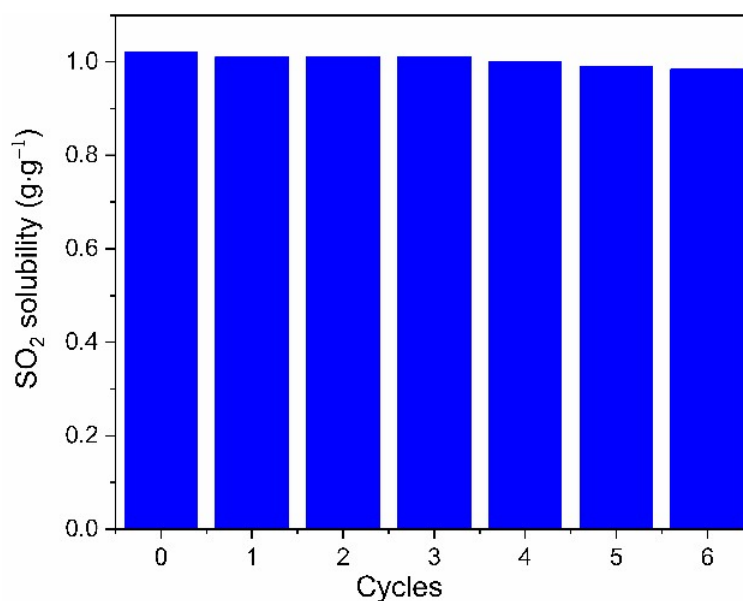
Regeneration of Eim-Im (1:1)

Fig. S23 Regeneration performance of Eim-Im (1:1) during SO_2 absorption/desorption cycles. Absorption: 298.2 K and 1.0 bar; Desorption: 333.2 K and 0.01 bar for 1.0 h.

The absorption capacity of SO_2 of Eim-Im (1:1) in six cycles is 1.02, 1.00, 1.00, 1.00, 0.993, 0.985, and 0.980 $g·g^{-1}$, respectively. To figure out the reason for the loss of absorption, a certain amount of Eim-Im (1:1) (about 1.61 g) was taken for the weight loss experiment under desorption conditions (333.2 K and 0.01 bar for 1.0 h), and the mass loss is only about 0.17%. However, the absorption capacity of the first cycle was 98 % of that of fresh DES in the regeneration experiment. Thus the slight loss of SO_2 capacity should be attributed to the strong chemical interaction between SO_2 and Eim-Im (1:1), resulting in the incomplete release of SO_2 during desorption, rather than the volatilization of Eim-Im (1:1).

Table S4. A summary of CO_2 and N_2 solubilities in HPLs at 313.2 K and 1.0 bar.

HPLs	CO_2 ($g·g^{-1}$)	N_2 ($*10^{-4}$ $g·g^{-1}$)
NMP-2-Pyr (1:1)	0.0196	2.93
Eim-Im (1:1)	0.0175	1.47
DMU-TMU (1:2)	0.0200	

AA-MAA (1:3)	0.0144
2-Iml-DMI (1:3)	0.0167

The calculation of ideal selectivities

$$S_{SO_2/CO_2} = \frac{W_{SO_2}}{W_{CO_2}} \tag{2}$$

$$S_{SO_2/N_2} = \frac{W_{SO_2}}{W_{N_2}} \tag{3}$$

where W_{SO_2}, W_{CO_2}, and W_{N_2} denote the absorption capacities of SO_2, CO_2, and N_2 in the unit of g·g^{-1} at 313.2 K and 1.0 bar, respectively. S_{SO_2/CO_2} and S_{SO_2/N_2} are utilized to estimate the ability of these HPLs for selectively separating of SO_2 from CO_2 and N_2, respectively.
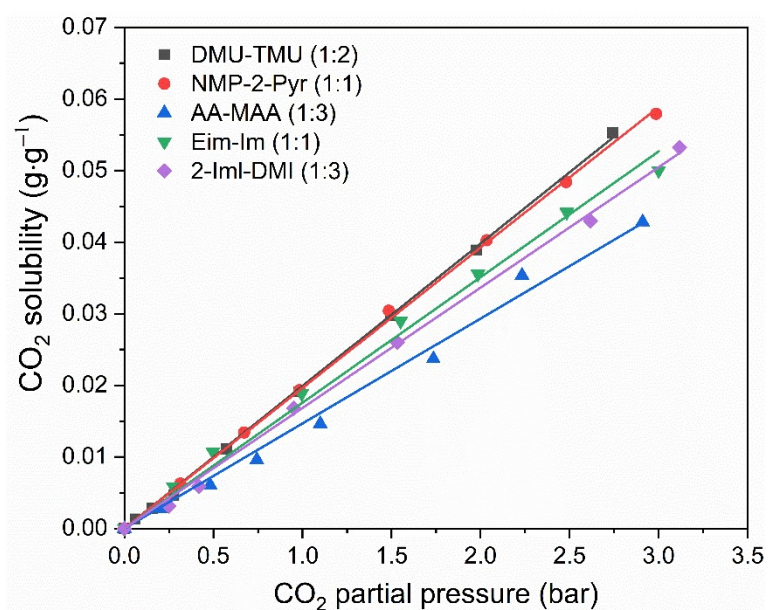

Figure S24. CO_2 solubility as a function of pressure in five HPLs at 313.2 K.

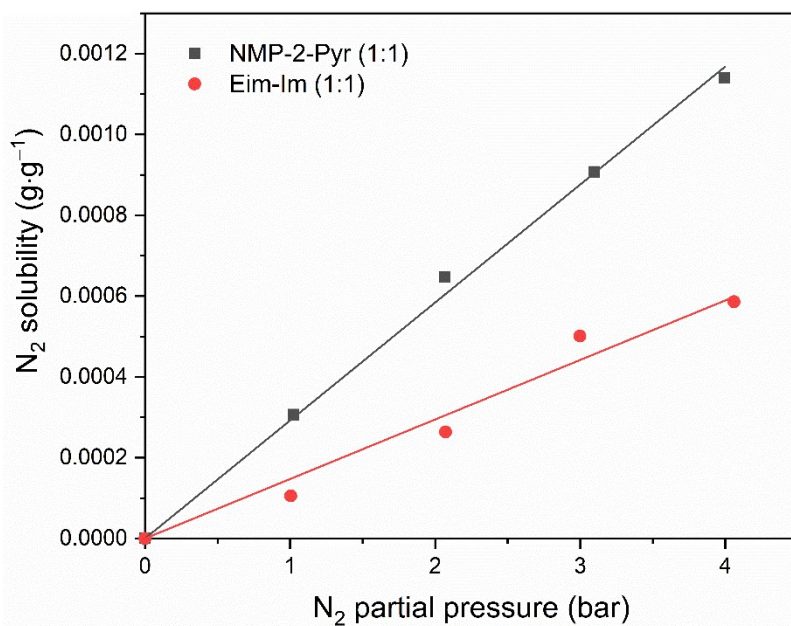**Figure S25**. N_2 solubility as a function of pressure in NMP-2-Pyr (1:1) and Eim-Im (1:1) at 313.2 K.

Table S5. Comparison of HPLs with DESs, ILs, and conventional organic solvents in the absorption of SO_2.

DESs	Temperature (K)	Viscosity (mPa·s)	SO_2 solubility at 1.0 bar (g·g^{-1})	References
NMP-2-Pyr (1:1)	298.2 (313.2)	4.71 (3.42)	0.89 (0.63)	This work
Eim-Im (1:1)	298.2 (313.2)	5.45 (3.66)	1.02 (0.77)	This work
ChCl-Glycerol (1:2)	313.2	~100	0.26	[4]
TEAC-Levulinic acid (1:3)	313.2	NA	0.36	[5]
Acetamide–KSCN (3:1)	313.2	20.3	0.37	[6]
EmimCl-NFM (1:1)	313.2	79.4	0.16 [a]	[7]
Betaine-EG (1:3)	313.2	NA	0.37 [b]	[8]
Ethylenurea-BMIMCl (1:2)	303.2	375.9	0.95	[9]
Caprolactam-Acetamide (1:1)	313.2	66.5 [c]	0.62	[10]
ChCl-Guaiacol (1:3)	313.2	~140	~0.3	[11]
BmimCl-Imidazole (1:1)	293.2	345.3 [d]	1.29	[12]
[N$_{2222}$][Cl]-EG (1:2)	293.2	NA	0.79	[13]
[Bmim][BF$_4$]	313.2	48.9 [14]	0.23	[5]
[Bmim][Ac]	298.2	133 [e]	0.62	[15]
[N$_{2224}$][dimaleate]	313.2	273 [f]	0.41	[16]

[TMG][Lac]	313.2	NA	0.31	17
[C$_4$Py][SCN]	313.2	42.0	0.65	5
[P$_{66614}$][Tetz]	293.2	NA	0.43	18
TEACl-Im (1:3)	293.2	139	1.25	19
Methanol	298.2	0.45 [b]	0.59	20
Acetone	298.2	0.27 [b]	0.87	20
Ethyl acetate	298.2	0.36 [b]	0.52	20
NDI	313.2	13.3	0.38	21
Sulfolane	313.2	7.30 [b]	0.29	22
Ethylene glycol	313.2	25.7 [g]	0.14	22
Propylene carbonate	313.2	2.5 [h]	0.25	22
Tetraethylene glycol dimethyl	313.2	2.32 [b]	0.36 [i]	23

[a] 10000 ppm; [b] from Chemical Properties Handbook; [c] at 303.2 K; [d] at 298.2 K; [e] at 313.2 K; [f] at 298.2 K; [g] at 289.2 K; [h] at 298.2 K.; [i] 0.925 bar; NA: not available.

References

1. D. S. Deng, X. B. Liu and B. Gao, *Ind. Eng. Chem. Res.*, 2017, **56**, 13850-13856.

2. P. Zhang, W. Xiong, M. Shi, Z. Tu, X. Hu, X. Zhang, and Y. Wu, *Chem. Eng. J.*, 2022, **438**, 135626.

3. Z. Li, L. Zhou, Y. Wei, H. Peng, and K. Huang, *Ind. Eng. Chem. Res.* 2020, **59**, 13696−13705.

4. D. Z. Yang, M. Q. Hou, H. Ning, J. L. Zhang, J. Ma, G. Y. Yang and B. X. Han, *Green Chem.*, 2013, **15**, 2261-2265.

5. D. S. Deng, G. Q. Han and Y. T. Jiang, *New J. Chem.*, 2015, **39**, 8158-8164.

6. B. Liu, F. Wei, J. Zhao and Y. Wang, *RSC Adv.*, 2013, **3**, 2470-2476.

7. D. Deng, C. Zhang, X. Deng and L. Gong, *Energy Fuels*, 2020, **34**, 665-671.

8. K. Zhang, S. H. Ren, Y. C. Hou and W. Z. Wu, *J. Hazard. Mater.*, 2017, **324**, 457-463.

9. B. Jiang, H. M. Zhang, L. H. Zhang, N. Zhang, Z. H. Huang, Y. Chen, Y. L. Sun and X. W. Tantai, *ACS Sustainable Chem. Eng.*, 2019, **7**, 8347-8357.

10. B. Y. Liu, J. J. Zhao and F. X. Wei, *J. Mol. Liq.*, 2013, **180**, 19-25.

11. X. B. Liu, B. Gao and D. S. Deng, *Sep. Sci. Technol.*, 2018, **53**, 2150-2158.

12. Y. Chen, B. Jiang, H. Z. Dou, L. H. Zhang, X. W. Tantai, Y. L. Sun and H. M. Zhang, *Energy Fuel.*, 2018, **32**, 10737-10744.

13. G. Cui, D. Yang and H. Qi, *Ind. Eng. Chem. Res.*, 2021, **60**, 4536-4541.

14. X. Zhang, Z. Tu, H. Li, K. Huang, X. Hu, Y. Wu and D. R. MacFarlane, *J. Membrane Sci.*, 2017, **543**, 282-287.

15. M. B. Shiflett and A. Yokozeki, *Ind. Eng. Chem. Res.*, 2010, **49**, 1370-1377.

16. K. Huang, G.-N. Wang, Y. Dai, Y.-T. Wu, X.-B. Hu and Z.-B. Zhang, *RSC Adv.*, 2013, **3**, 16264-16269.

17. W. Wu, B. Han, H. Gao, Z. Liu, T. Jiang and J. Huang, *Angew. Chem. Int. Ed.*, 2004, **43**, 2415-2417.

18. C. Wang, G. Cui, X. Luo, Y. Xu, H. Li and S. Dai, *J. Am. Chem. Soc.*, 2011, **133**, 11916-11919.

19. P. Zhang, G. Xu, M. Shi, Z. Wang, Z. Tu, X. Hu, X. Zhang and Y. Wu, *Sep. Purif. Technol.*, 2022, **286**, 120489.

20. W. Hayduk and H. Pahlevanweh, *Can. J. Chem. Eng.*, 1987, **65**, 299-307.

21. K. Huang, Y.-L. Chen, X.-M. Zhang, S.-L. Ma, Y.-T. Wu and X.-B. Hu, *Fluid Phase Equilibr.*, 2014, **378**, 21-33.

22. K. Huang, S. Xia, X.-M. Zhang, Y.-L. Chen, Y.-T. Wu and X.-B. Hu, *J. Chem. Eng. Data*, 2014, **59**, 1202-1212.

23. K. A. G. Schmidtt and A. E. Mather, *Can. J. Chem. Eng.*, 2001, **79**, 946-960.